LAWRENCE
LIVERMORE
NATIONAL
LABORATORY

LLNL-JRNL-668928

Effect of Multiple Scattering on the Compton Recoil Current Generated in an EMP, Revisited

W. A. Farmer, A. Friedman

March 25, 2015

IEEE TRANSCATIONS ON NUCLEAR SCIENCE

Disclaimer

Effect of Multiple Scattering on the Compton Recoil Current Generated in an EMP, Revisited

William A. Farmer and Alex Friedman

***Abstract*—Multiple scattering has historically been treated in EMP modeling through the obliquity factor. The validity of this approach is examined here. A simplified model problem, which correctly captures cyclotron motion, Doppler shifting due to the electron motion, and multiple scattering is first considered. The simplified problem is solved three ways: the obliquity factor, Monte-Carlo, and Fokker-Planck finite-difference. Because of the Doppler effect, skewness occurs in the distribution. It is demonstrated that the obliquity factor does not correctly capture this skewness, but the Monte-Carlo and Fokker-Planck finite-difference approaches do. The obliquity factor and Fokker-Planck finite-difference approaches are then compared in a fuller treatment, which includes the initial Klein-Nishina distribution of the electrons, and the momentum dependence of both drag and scattering. It is found that, in general, the obliquity factor is adequate for most situations. However, as the gamma energy increases and the Klein-Nishina becomes more peaked in the forward direction, skewness in the distribution causes greater disagreement between the obliquity factor and a more accurate model of multiple scattering.**

***Index Terms*—EM analysis, EMP radiation effects, high altitude electromagnetic pulse (HEMP), nuclear explosions, radiative interference**

I. Introduction

THE theory to describe a nuclear electromagnetic pulse (EMP) was developed over 40 years ago by Longmire [1]–[4] and Karzas and Latter [5], [6]. This theoretical treatment describes the Compton production of energetic electrons due to the gamma ray output of a nuclear explosion. These Compton electrons then bend in the earth's magnetic field and radiate an electromagnetic signal. Because the gamma pulse propagates at the speed of light, the radiation from the many Compton electrons at differing altitudes adds coherently, resulting in a large propagating wave signal far from the source region. The Compton electrons interact with the background atmosphere through collisions with background electrons and nuclei. As the background electrons slow the Compton electrons, the background atmosphere becomes ionized, giving a finite conductivity to the background medium. This leads to dissipation of the pulse due to Ohmic losses. Collisions between the Compton electrons and the background nuclei primarily deflect the fast electron through small angles, and the gradual energy loss by the electron is due to drag forces on background electrons.

These effects are modeled in the geomagnetic EMP code, CHAP [7]. Motivated by computational limitations at the time of development, an elegant simplification to model the effects of multiple scattering by the background nuclei was proposed [8]. Instead of performing a Monte-Carlo treatment of the collisional scattering with many electrons, each electron in CHAP describes the center of a distribution that is diffusing in velocity space. Consider an energetic electron propagating in the z direction which is only experiencing forces due to scattering collisions with the background. In a time interval, dt, the total distance travelled by the electron, ds, is related to the distance travelled along the z axis, dz, through

$$dz = ds\cos\theta, \tag{1}$$

where θ is the angle through which the electron has been scattered. If a statistical average is then performed over all possible scattering angles,

$$\langle dz\rangle = ds\,\langle\cos\theta\rangle = \frac{ds}{\eta}, \tag{2}$$

where the obliquity factor, $\eta = 1/\langle\cos\theta\rangle$, has been introduced. The appellation, obliquity factor, was originally chosen because it is used to describe the decrease in average path length in a time step due to obliquely traveling electrons. Dividing by the time interval, the average velocity of the distribution is

$$v_{\text{eff}} = \left\langle\frac{dz}{dt}\right\rangle = \frac{v}{\eta}. \tag{3}$$

From the above expression, it is seen that the velocity is reduced by a factor of $1/\eta$ to an effective velocity. This occurs because particles scattered from the initial direction move a smaller distance along the z axis causing the average displacement in the z direction to lag behind the displacement of an unscattered particle. For an electron with momentum, $\mathbf{p}$, and absolute charge, e, which is interacting with electric and magnetic fields, $\mathbf{E}$ and $\mathbf{B}$, respectively, the equations of motion in the obliquity factor formulation are

$$\frac{d\mathbf{p}}{dt} = -e\left(\mathbf{E} + \frac{\mathbf{v}}{c}\times\mathbf{B}\right), \tag{4}$$

$$\frac{d\mathbf{r}}{dt} = \frac{\mathbf{v}}{\eta}, \tag{5}$$

$$\frac{d\eta}{dt} = \left[\frac{1}{2}\frac{d\left\langle\theta^2\right\rangle}{dt} + e\left(\eta^2-1\right)\frac{\mathbf{E}\cdot\mathbf{p}}{p^2}\right]\eta. \tag{6}$$

The last equation above is derived in [2] and [8]. Here, $d\left\langle\theta^2\right\rangle/dt$ is the rate of increase in the variance of the angle, θ, and is given by the underlying collisional process. The second term arises due to the component of the electric field parallel to the momentum of the particle and is unimportant for the development of this paper. It is included here for completeness.

The authors are with Lawrence Livermore National Laboratory, Livermore, CA 94551 USA.

Manuscript received [Month Day, Year]; revised [Month Day, Year]. This work was supported by the U.S. Department of Energy by Lawrence Livermore National Laboratory under Contract DE-AC52-07NA27344

Because the outgoing gamma pulse is traveling at the speed of light, it is useful to perform a variable transformation, so that the equations are expressed in terms of the time since the gamma front has passed a given position. If the gamma pulse is propagating in the z direction, then this is done through the substitution, $\tau = t - z/c$. This substitution results in a decoupling of the fast time scale associated with the gamma pulse and the much smaller spatial variations, e.g., changes in atmospheric density. Further, for an observer at a fixed position, τ is equivalent to t measured from the time from which the gamma pulse would first arrive at the observer. This transformation is most easily understood as a Doppler shift due to a moving source and should not be confused with a Lorentz transformation. All quantities exist in the same reference frame, i.e., that of the observer. When applied to the equations of motion for the electron, temporal derivatives are transformed through

$$f_r \frac{d}{dt} = \frac{d}{d\tau}, \tag{7}$$

$$f_r = \frac{1}{\left(1 - \frac{v_z}{c}\right)}. \tag{8}$$

Having initialized a distribution of electrons with momenta, $\mathbf{p}_i$, and obliquity factor, η_i, the current density is given by

$$\mathbf{j} = -e \sum_i W_i \frac{\mathbf{v}_i/\eta_i}{1 - v_{z,i}/c\eta_i}. \tag{9}$$

Here, W_i is a weight function which corresponds to the number of Compton electrons created per unit volume at that given initial velocity and is determined by the cross section.

In addition to finding the Compton current, CHAP also determines the conductivity of the background due to ionizing collisions occurring between the Compton electrons and the background, and then uses both the Compton current and the conductivity to solve Maxwell's equations for the fields [7]. Assuming a planar geometry with symmetry in the transverse coordinates, Maxwell's equations reduce to a one-dimensional wave equation, which takes the following form [3],

$$\frac{1}{2}\frac{\partial F}{\partial z} + \frac{\pi\sigma}{c}F = -\frac{2\pi}{c}j_x - \frac{\pi\sigma}{c}G, \tag{10}$$

$$\frac{1}{c}\frac{\partial G}{\partial \tau} + \frac{\pi\sigma}{c}G = \frac{1}{2}\frac{\partial G}{\partial z} - \frac{2\pi}{c}j_x - \frac{\pi\sigma}{c}F, \tag{11}$$

where the equations have been expressed in the (τ, z) coordinate system. Here, σ is the background air conductivity, and $F = E_x + B_y$ and $G = E_x - B_y$ represent the outgoing and incoming waves, respectively. Consistent with standard EMP analysis, it is assumed that $G \ll F$ or that $E_x \approx B_y$. With this approximation, the transverse electric field is found to be

$$E_x = -\frac{2\pi}{c}\int_{-\infty}^{z} j_x(z', \tau) e^{-\frac{2\pi}{c}\int_{z'}^{z}\sigma(z'',\tau)dz''} dz'. \tag{12}$$

In this manuscript, the conductivity is set to zero. This is done in order to clarify the dynamics of the Compton current and to determine the accuracy of the obliquity factor formulation of multiple scattering. Under this approximation, the electric field is proportional to the integral of the current density over altitude. For this reason, the rise-time of the current density is closely related to the rise time of the field seen by the observer. This may seem counterintuitive as typically the radiated field is related to the time derivative of the current density and not the current density itself. However, as Longmire showed [4], when one integrates the single-particle radiated field over the distributed emitters in the transverse direction, this is equivalent to integrating with respect to time. As a consequence, the electric field is proportional to the current density.

This relation between the Compton current and the radiated field changes when conductivity is included in the model, and the EMP fields can become saturated. If the spatial scale length over which the atmospheric parameters vary is defined as L_z, then saturation occurs when

$$\frac{2\pi\sigma(\tau, z)L_z}{c} \gg 1. \tag{13}$$

In this limit, the spatial gradients are negligible, and the solution becomes

$$E_x \approx -\frac{j_x(t - z/c)}{\sigma(t - z/c)}. \tag{14}$$

The above equation is a solution to the one-dimensional homogeneous wave equation. Thus, when saturation occurs, the Compton current, having been cancelled by the conduction current, is no longer sourcing the radiated field. To make accurate rise-time predictions for the fields, a conductivity model must be included in the description of the fields, unless a low-yield (also a low EMP field) case in which saturation does not occur is considered. The process of field attenuation is beyond the scope of this paper, which is restricted to assessing differences between the computed Compton current by the obliquity factor model and a more fundamental description of multiple scattering.

Comparisons between the obliquity factor and a Monte-Carlo method have been performed previously [8]–[10]. Knutson [9] first developed a Monte-Carlo approach in which the particles are tracked in the coordinates, (x, y, z, t). The particles in his simulation experience forces due to the background magnetic field, an average drag on the background electrons, and the scattering off of background nuclei. The effects of the EMP fields on the particle motion are neglected, so the simulation is not self-consistent, a simplification which is also made in this manuscript. This is appropriate because the Compton current is not sensitive to the self-consistent inclusion of the Lorentz force caused by the EMP fields [11]. Three random numbers are used to determine the following: the distance propagated between scatters, the pitch angle scattered from the incident direction, and the azimuthal deflection of the resulting scatter. The current density is then computed in τ, and comparisons are made to obliquity factor predictions. The initial distribution of electrons is taken to be a single, forward-traveling electron with the average energy of the Klein-Nishina distribution for a given gamma ray energy. This work was later generalized by Morgan and Knutson [10] to include the full Klein-Nishina distribution. Longmire similarly performed a comparison between a Monte-Carlo calculation and obliquity factor predictions [8]. The details of Longmire's Monte-Carlo simulation never seem to have been published.

However, because he references Knutson's work, it is assumed that he used a similar approach to that of Knutson [9]. From this comparison, Longmire determined that the two methods agree to within two or three percent of the correct value.

Out of these Monte-Carlo studies, another legacy code, HEMP-B, was developed which includes both Monte-Carlo and obliquity factor models [12]. Figure 6 in this reference illustrates a typical, highly-saturated EMP scenario, comparing the obliquity factor model and a Monte-Carlo model. In this case, the curves agree closely until roughly 5 ns after the peak has occurred, at which point they diverge. High saturation implies that the effects of conductivity become large early in the rise of the pulse. This suggests that the obliquity factor is adequate if large saturation occurs.

Contemporary with Longmire and Knutson, Vajk [13] also performed Monte-Carlo studies of multiple scattering in EMP. Vajk observed that, in the coordinate, τ, electrons experience differential rotation and shear due to the factor, f_r, that appears in (7). This occurs because, for a given time step, $d\tau$, more electron time, dt, elapses for electrons moving along the z-axis than those moving obliquely. Thus, for a given $d\tau$, more scatters occur for electrons near the z-axis. This results in a skewed distribution, shifting the average particle momentum. In mentioning the previous Knutson work, Vajk attributes the agreement between Monte-Carlo and the obliquity factor models to only using the averaged Klein-Nishina distribution, but this was only true in the first report [9] and not the second [10]. In referring to Vajk's work, Longmire was critical because the initial value of the current density computed by Vajk is not the same for both approaches [3]. For this reason, it is difficult to conclude from Vajk's work how the two methods differ.

Since this time, it has widely been accepted that the obliquity factor is adequate for most practical calculations. Recently, Kruger [14] performed simulation studies of EMP. In his work, the subroutine MCNP [15] was called to transport the gamma rays and Compton electrons. From his main code, MACSYNC, he computed the synchrotron radiation of the Compton electrons at the observer using the Liénard-Wiechert fields. In performing this calculation, Kruger made two approximations. First, the cyclotron motion of the electrons was not included in the electron transport. This is most appropriate at ground level, because the range of the electron due to drag forces is much less than the cyclotron radius. Second, the Liénard-Wiechert fields only include the synchrotron radiation, and not that due to deceleration caused by collisions. Kruger argued that the radiation due to these deceleration terms cancel in the absence of asymmetries. Under these assumptions, Kruger placed a lower-limit on the rise times of the EMP that is an order of magnitude longer than those predicted by CHAP. He attributed this to the obliquity factor's approximate treatment of multiple scattering and suggests that a proper description of multiple scattering would lengthen the rise times of an EMP pulse.

In light of the above works, it is the aim of this paper to determine the impact of multiple scattering on the Compton current created during a nuclear explosion. For this reason, a Fokker-Planck equation is used to model the dynamic evolution of the distribution of Compton electrons. This approach is adopted not for numerical efficiency, but because it gives insight that could lead to an efficient and accurate particle-based approach. This manuscript is organized as follows. In section II, the basic theory of EMP is formulated in a Fokker-Planck equation. For general interest, a semi-analytic solution of the full problem that neglects collisions is presented in the Appendix. Section III then simplifies the problem to one that contains all of the salient features of the general problem that are necessary to understanding multiple scattering. Three numeric approaches are presented in III-A: the obliquity factor, Monte-Carlo, and a finite-difference scheme. Results are presented in III-B, and a discussion of the three approaches is given. Section IV then develops the numerical machinery to solve the full problem, and results for realistic parameters are presented. Finally, major conclusions are presented in Section V, and these results are placed in context with previous work.

II. Fokker-Planck approach to EMP

We first assume an impulse of gamma rays with number density, n_γ, given by

$$n_\gamma = N_\gamma \delta\left(z - ct\right). \tag{15}$$

Here, the gamma pulse is described by a delta function with the number of gamma photons per unit area given by N_γ. The gamma photons scatter background electrons as described by the Klein-Nishina cross section, creating a source term in the kinetic equation governing the Compton electrons. The dynamic evolution of the distribution of gamma rays is neglected, and as a result, this source term is translationally invariant with respect to the coordinate, $\tau = t - z/c$. Because of this, the source term can be included by specifying the initial distribution of Compton electrons, f_0, to be

$$f(\tau = 0, \mathbf{p}) = f_0(\mathbf{p}) = \frac{Z n_i N_\gamma}{1 - v_z/c} \frac{\delta(p - p_0(\psi))}{p^2} \sigma_{KN}. \tag{16}$$

Here, $Z = 7.2$ is the mean atomic number of air, and n_i is the atomic number density. The Klein-Nishina differential cross section is given by σ_{KN}. Traditionally, it is expressed in terms of $\chi = 1 - \cos\zeta$, where ζ is the scattered angle of the incident photon. Since the electron motion is of greater concern here, the cross section is expressed in terms of the ejection angle of the electron, ψ, measured from the direction of photon incidence. This takes the form,

$$\begin{aligned} \sigma_{KN} = {} & \frac{r_0^2}{2} \frac{1}{\left(1 + g\chi(\psi)\right)^2} \frac{1}{\sin\psi} \left|\frac{d\chi}{d\psi}\right| \\ & \times \left[1 + \left(1 - \chi(\psi)\right)^2 + \frac{g^2 \chi(\psi)^2}{1 + g\chi(\psi)}\right], \end{aligned} \tag{17}$$

$$\chi(\psi) = \frac{2\cos^2\psi}{1 + g(2+g)\sin^2\psi}, \tag{18}$$

$$\frac{p_0(\psi)}{mc} = \frac{g}{1 + g\chi(\psi)} \sqrt{\chi(\psi)\left[2 + g\chi(\psi)(2+g)\right]}. \tag{19}$$

In the above expressions, $g = E_\gamma/mc^2$ is the ratio of the photon energy to the electron rest mass, and $r_0 = e^2/mc^2$ is the classical electron radius. Because we have chosen to use the ejection angle of the electron, it should be noted that

ψ is restricted to the range $0 \leq \psi \leq \pi/2$. This is because the scattering process cannot eject the electron opposite the direction of the incident photon and still conserve momentum and energy.

Once the Compton electrons are created, a kinetic equation describes their resulting motion. Assuming that collisions are frequent but only cause small changes in the momentum of a fast electron, a Fokker-Planck equation can be used [16], which is of the form

$$\frac{\partial f}{\partial t}+\mathbf{v}\cdot\frac{\partial f}{\partial \mathbf{r}}+\mathbf{F}\cdot\frac{\partial f}{\partial \mathbf{p}}=-\frac{\partial}{\partial \mathbf{p}}\cdot(\mathbf{a}f)+\frac{\partial}{\partial p_i}\cdot\left(D_{i,j}\frac{\partial f}{\partial p_j}\right). \quad (20)$$

Here, $\mathbf{F}$ is the full electromagnetic force on the electrons. To be self-consistent, this force must include contributions from the EMP-field generated by the Compton current and from the conduction current of secondary electrons. Since the effects of multiple scattering and turning in the magnetic field are of primary interest, only the force due to the background magnetic field is retained, so that

$$\mathbf{F}=-\mathbf{p}\times\mathbf{\Omega}, \quad (21)$$

where $\mathbf{\Omega}=e\mathbf{B}/mc\gamma$ is the relativistic cyclotron frequency. The drag and diffusion forces are given by $\mathbf{a}$ and $D_{i,j}$, respectively. The drag coefficient is given by the Bethe formula [17],

$$\mathbf{a}=-mc\frac{\omega_{pe}^2 r_0}{c}\left(\frac{mc\gamma}{p}\right)^2 L_D\frac{\mathbf{p}}{p}, \quad (22)$$

$$L_D=\log\left(\frac{E\sqrt{\gamma+1}}{I}\right)-\frac{1}{2}\log 2+\frac{1}{16}+\frac{(\log 2)/2+9/16}{\gamma^2}-\frac{\log 2+1/8}{\gamma}. \quad (23)$$

The frequency, $\omega_{pe}=\sqrt{4\pi Z n_i e^2/m}$, is analogous to the plasma frequency, except that Zn_i is the number density of background electrons, including those in bound atomic states. Additionally, γ is the familiar relativistic factor for the Compton electron, $E=mc^2(\gamma-1)$ is the corresponding kinetic energy, and I is the mean excitation potential of a bound electron, which we take to be $I=80.5$ eV. The density effect [17] is not included in the above expressions, because it is not present in air.

Next, we consider the diffusive processes. Diffusion in the magnitude of momentum, or energy straggling, was neglected by Longmire [8]. He argued that in the source region, i.e. altitudes of 20-40 km, energy straggling would likely have little effect on the peak Compton current. Because we wish to compare to the obliquity factor model used by Longmire, this effect is ignored here. Further, the dominant source of angular diffusion is due to collisions with nuclei. Vajk includes electron collisions by replacing a factor of Z^2 with $Z(Z+1)$ [13], and concludes that this would increase the scattering rate by 12%. However, Longmire states that this procedure is not valid for small angle scattering where the atomic electrons are already included in the atomic screening [8]. For this reason, Longmire's approach is adopted, and the angular portion of the diffusion constant is taken to be

$$D=\frac{1}{4}\frac{d\left\langle\theta^2\right\rangle}{dt}. \quad (24)$$

In choosing an expression to model $d\left\langle\theta^2\right\rangle/dt$, modern formulas exist [17] that are more accurate than those initially used by Longmire [2]. However, since the goal is to make contact with Longmire's work, his choice is adopted, giving

$$\frac{d\left\langle\theta^2\right\rangle}{dt}=\frac{2Z\omega_{pe}^2 r_e}{c}\frac{c}{v}\left(\frac{m_e c}{p}\right)^2 L_S, \quad (25)$$

$$L_S=\log\left(\frac{131\sqrt{\gamma^2-1}}{Z^{1/3}}\right). \quad (26)$$

If we assume a constant air density, (20) can be simplified by observing that the distribution function can depend only on the coordinates τ and $\mathbf{p}$. Further, it is convenient to write $\mathbf{p}$ in spherical coordinates, (p,ψ,α), ψ and α being the polar and azimuthal angles, respectively. For computational purposes, instead of using ψ, the substitution $\mu=\cos\psi$ is performed. Finally, for definiteness, the background magnetic field is placed anti-parallel to the y-axis. This gives the equation,

$$\left(1-\frac{v_z}{c}\right)\frac{\partial f}{\partial \tau}+\Omega\left[\frac{\partial}{\partial\alpha}\left(\sin\alpha\frac{\mu}{\sqrt{1-\mu^2}}f\right)+\frac{\partial}{\partial\mu}\left(\cos\alpha\sqrt{1-\mu^2}f\right)\right]=\frac{1}{p^2}\frac{\partial}{\partial p}\left(ap^2 f\right)+D\left[\frac{\partial}{\partial\mu}\left((1-\mu^2)\frac{\partial f}{\partial\mu}\right)+\frac{\partial}{\partial\alpha}\left(\frac{1}{1-\mu^2}\frac{\partial f}{\partial\alpha}\right)\right]. \quad (27)$$

If the above equation is integrated with respect to the momentum coordinates, an equation for the Compton electron density, n_c, is found to be

$$\frac{d}{d\tau}\left(n_c-n_c\frac{\langle v_z\rangle}{c}\right)=0, \quad (28)$$

$$n_c=n_{c0}\frac{1-\langle v_z\rangle_0/c}{1-\langle v_z\rangle/c}. \quad (29)$$

In the above expressions, a zero subscript denotes an initial quantity, and angle brackets correspond to averages over the distribution.

If an auxiliary function is defined, $\tilde{f}=p^2 f$, so that factors of the Jacobian are absorbed into the distribution function, and the time coordinate is scaled to the non-relativistic cyclotron frequency, Ω_0, then (27) can be rewritten as

$$\left(1-\frac{p}{mc\gamma}\mu\right)\frac{\partial\tilde{f}}{\partial(\Omega_0\tau)}+\frac{1}{\gamma}\left[\sin\alpha\frac{\mu}{\sqrt{1-\mu^2}}\frac{\partial\tilde{f}}{\partial\alpha}+\cos\alpha\sqrt{1-\mu^2}\frac{\partial\tilde{f}}{\partial\mu}\right]=\frac{\partial}{\partial\left(p/mc\right)}\left(\kappa\tilde{f}\right)+\Lambda\left[\frac{\partial}{\partial\mu}\left((1-\mu^2)\frac{\partial\tilde{f}}{\partial\mu}\right)+\frac{1}{1-\mu^2}\frac{\partial^2\tilde{f}}{\partial\alpha^2}\right]. \quad (30)$$

Here, $\kappa=a/mc\Omega_0$ and $\Lambda=D/\Omega_0$; these parameters give the relative importance of drag and scatter to the advection caused by the cyclotron motion. To show scalings, these coefficients can be expressed as

$$\kappa=1.7\times10^{-21}\ \frac{Zn_i(\mathrm{cm}^{-3})}{B(\mathrm{Gauss})}\left(\frac{c}{v}\right)^2 L_D, \quad (31)$$

$$\Lambda=8.5\times10^{-22}\ \frac{Z^2 n_i(\mathrm{cm}^{-3})}{B(\mathrm{Gauss})}\frac{c}{v}\left(\frac{mc}{p}\right)^2 L_S. \quad (32)$$

Having numerically solved for $\tilde{f}$, the current density of the Compton electrons can then be obtained by taking moments of the distribution. These are given by the expression,

$$\mathbf{j}(\tau) = -ec \int_{-\pi}^{\pi} d\alpha \int_{-1}^{1} d\mu \int_{0}^{\infty} dp \ \frac{\mathbf{p}}{mc\gamma} \tilde{f}(\tau, \mathbf{p}). \tag{33}$$

III. Simplified Problem

Before proceeding with a numerical solution to (30), a simpler problem is first considered for the purpose of gaining insight. Consider, then, the equation,

$$\left(1 - \frac{v}{c}\cos\phi\right) \frac{\partial f}{\partial \tau} + \Omega \frac{\partial f}{\partial \phi} = D \frac{\partial^2 f}{\partial \phi^2}, \tag{34}$$

$$f(\tau = 0, \phi) = \delta(\phi) \tag{35}$$

Physically, this problem is the two-dimensional analog of the full problem with drag neglected. Further, the diffusion and advection coefficients, D and Ω, are set as independent parameters, and the complicated dependence on the magnitude of the particle's momentum is ignored.

If the diffusion is also ignored, the simplified problem can be solved via the method of characteristics. Omitting the details, the solution is

$$f = \delta\left[\phi - \Omega t(\tau, \phi)\right], \tag{36}$$

$$\Omega\tau = \Omega t - \frac{v}{c}\left[\sin\phi - \sin\left(\phi - \Omega t\right)\right]. \tag{37}$$

An analytic solution of t in terms of τ and ϕ is not possible due to the transcendental equation that appears. However, the analog of the current density for this problem can be computed. We do this for the component transverse to the initial velocity direction, because this is the component that radiates the corresponding electromagnetic signal seen by an observer. Ignoring the charge of the electron,

$$\begin{aligned} j_y &= v \int \sin(\phi) f d\phi, \\ &= \frac{1 - \frac{v}{c}}{1 - \frac{v}{c}\cos\phi_0(\tau)} v \sin\phi_0(\tau), \end{aligned} \tag{38}$$

$$\Omega\tau = \phi_0(\tau) - \frac{v}{c}\sin\phi_0(\tau). \tag{39}$$

The above expression for j_y is easily seen to be the product of two terms: the number density as described in (29), and the velocity of the electron in the y direction. Determining the time-to-peak, τ_0, of the transverse current density,

$$\Omega\tau_0 = \cos^{-1}\frac{v}{c} - \frac{v}{c}\sqrt{1 - \frac{v^2}{c^2}}. \tag{40}$$

This time-to-peak acts as a check on numerical solutions. In the limit that $1 - v/c \ll 1$, the time-to-peak takes the asymptotic form,

$$\Omega\tau_0 \sim \frac{2}{3}\left[2\left(1 - \frac{v}{c}\right)\right]^{3/2}. \tag{41}$$

In Subsec. III-A, three different methods of solving (34) with diffusion included are outlined: the obliquity factor, Monte-Carlo, and finite difference. Comparisons between solutions from the three methods are then compared in Subsec. III-B, and a discussion is given.

A. Solution Approaches

To use a particle approach, equations governing ϕ and $\langle\phi^2\rangle$ are needed. Examining (34), these are

$$\frac{d\phi}{d\tau} = \frac{\Omega}{1 - \frac{v}{c}\cos\phi}, \tag{42}$$

$$\frac{d\langle\phi^2\rangle}{d\tau} = \frac{2D}{1 - \frac{v}{c}\cos\phi}. \tag{43}$$

A factor of two appears in (43), as opposed to the factor of four in (24), because this problem has two spatial dimensions instead of three. If the obliquity factor is used to model the distribution of electrons, the equations become

$$\frac{d\phi}{d\tau} = \frac{\Omega}{1 - \frac{v}{c\eta}\cos\phi}, \tag{44}$$

$$\frac{d\eta}{d\tau} = \frac{D}{1 - \frac{v}{c\eta}\cos\phi}\eta. \tag{45}$$

If the two equations are divided, the solution for the obliquity factor in terms of $\phi(\tau)$ is found to be

$$\eta = \exp\left(\frac{D\phi}{\Omega}\right). \tag{46}$$

Substituting the above expression into (44) and solving,

$$\Omega\tau = \phi - \frac{v}{c}\frac{\left[e^{-D\phi/\Omega}\sin\phi + D/\Omega\left(1 - e^{-D\phi/\Omega}\cos\phi\right)\right]}{D^2/\Omega^2 + 1}, \tag{47}$$

which generalizes (39). The expression for the transverse current density is

$$\begin{aligned} j_y &= \frac{1 - \frac{v}{c}}{1 - \frac{v}{c\eta}\cos\phi}\frac{v\sin\phi}{\eta}, \\ &= \frac{1 - \frac{v}{c}}{\exp\left(\frac{D\phi}{\Omega}\right) - \frac{v}{c}\cos\phi} v\sin\phi, \end{aligned} \tag{48}$$

where, as before, the number density is multiplied by the effective velocity in the first line. The second line has been written in terms of ϕ, where (46) has been used for η. The transverse current density can now be plotted parametrically using (48) and (47) for $j_y(\phi)$ and $\tau(\phi)$, respectively. Computing the angle at which the maximum transverse current density occurs, ϕ_{Max},

$$\cos\phi_{Max} - \frac{D}{\Omega}\sin\phi_{Max} = \frac{v}{c}\exp\left[-\frac{D\phi_{Max}}{\Omega}\right]. \tag{49}$$

The time-to-peak can then be determined by solving the above equation and then evaluating (47).

A Monte-Carlo approach is performed by implementing a first-order Euler-Maruyama scheme with a large number of particles, typically 10^5. The scheme is given by

$$\phi^{m+1} = \phi^m + \Delta\tau\left(\frac{d\phi}{d\tau}\right)^m + \sigma^m r^m, \tag{50}$$

where m is an index associated with the τ discretization, and $\Delta\tau$ is the time step, so that $\tau = m\Delta\tau$. The advective part of the equation is contained in the second term on the right hand side, and the scattering term, in the third. The value, r^m, is

a random number from a unit normal distribution, and σ^m is given by

$$\sigma^m = \sqrt{\frac{2D\Delta\tau}{1-\frac{v}{c}\cos\phi^m}}. \tag{51}$$

Each particle is initialized so that it is traveling in the x direction, i.e. $\phi(0) = 0$. Further, for N particles, the weight of each particle is given by $W = 1/N$. For this method, the current density is

$$\mathbf{j} = \sum_n W \frac{1-\frac{v}{c}}{1-\frac{v}{c}\cos\phi_n}\mathbf{v}_n, \tag{52}$$

and can be computed at each time step.

A finite-difference method for (34) is implemented by using an upwind difference for the advection term and a centered difference for the diffusion term. This takes the form

$$\frac{\partial f_i}{\partial\tau} = \sum_j A_{i,j} f_j, \tag{53}$$

$$A_{i,j} = \begin{cases} \left(1-\frac{v}{c}\cos\phi_i\right)^{-1}\left(D/h^2+\Omega/h\right), & j=i-1 \\ -\left(1-\frac{v}{c}\cos\phi_i\right)^{-1}\left(\frac{2D}{h^2}+\frac{\Omega}{h}\right), & j=i \\ \left(1-\frac{v}{c}\cos\phi_i\right)^{-1}\frac{D}{h^2}, & j=i+1 \\ 0, & \text{otherwise} \end{cases}, \tag{54}$$

with periodic boundary conditions in ϕ. Crank-Nicholson is then used to advance in time. The distribution function is initialized as a Gaussian with unit area and standard deviation of one degree in order to approximate the delta function. In the ϕ discretization, 400 points are used in order to resolve the initial function. Finally, in this approach, the current density is computed by numerically evaluating the integral,

$$\mathbf{j} = \int \mathbf{v} f(\phi,\tau)\, d\phi. \tag{55}$$

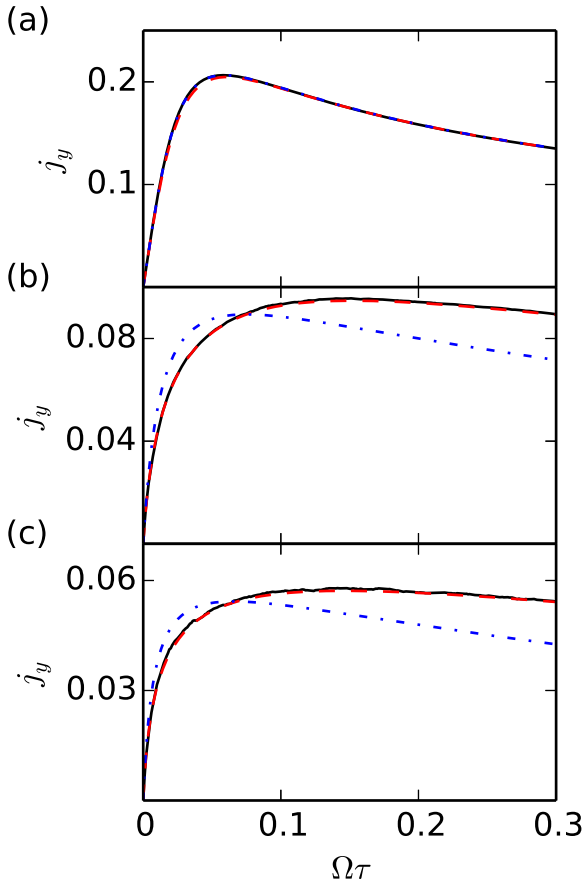

Fig. 1. Transverse current density for simplified problem. Performed at three different values of D/Ω: (a) 0, (b) 0.5, and (c) 1.0. Black solid, red dashed, and blue dash-dotted curves correspond to Fokker-Planck, Monte-Carlo, and obliquity factor approaches.

B. Results and Discussion

Using the three different approaches described above, j_y is computed for $v/c = 0.9$ with three different values of D/Ω in Fig. 1. The top, middle, and bottom panels correspond to $D/\Omega = 0$, 0.5, and 1.0, respectively. The solid black curves, dashed red curves, and dash-dotted blue curves correspond to solutions generated via the Fokker-Planck, Monte-Carlo, and obliquity factor methods, respectively. The vertical axes in each panel correspond to j_y. The range on this axis decreases as D/Ω increases, reflecting the decrease in the maximum current value due to increased spreading of the electrons over a larger range of ϕ. In all three panels, the Monte-Carlo and Fokker-Planck solutions agree almost identically. For the number of particles used, the noise in the Monte-Carlo solutions is not visible, but it is present. The obliquity factor agrees qualitatively in panels (b) and (c), but it rises and falls more rapidly than the other two approaches.

In an effort to quantify the differences between the approaches, the time to the peak of the signal is plotted for the Fokker-Planck and obliquity factor methods in Fig. 2. The time-to-peak for the Monte-Carlo method is not plotted because it has a large degree of fluctuation. This is caused by the noise inherent in Monte-Carlo methods and the flatness of the peak that occurs when $D/\Omega \sim 1$. The vertical axis in the figure corresponds to the time-to-peak, τ_{Max}, relative to the time-to-peak when no diffusion is present, τ_0, given in (40). For our choice of velocity, $\Omega\tau_0 = 5.87\times10^{-2}$. The horizontal axis corresponds to the relative diffusion, D/Ω. The solid and dashed curves correspond to the time-to-peak computed from the obliquity factor and Fokker-Planck approaches, respectively. It is seen that both signals rise and fall as the diffusion increases, but that the Fokker-Planck time-to-peak can exceed that given by the obliquity factor by roughly a factor of two or more. Further, this difference remains even at large values of D/Ω.

In assessing the differences between the two approaches, it is first useful to understand why the obliquity factor model exhibits a rise and fall in the time-to-peak. As the diffusion constant increases, both the effective velocity, v/η, and the density of the electrons decrease more rapidly due to the spreading of the distribution in the ϕ coordinate. This causes a monotonic decrease in the angle, ϕ_{Max}, at which the transverse current peaks. If the electron rotation frequency was independent of the diffusion rate, this would cause the

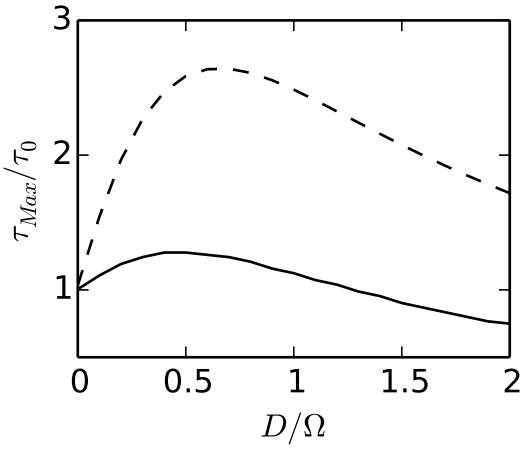

Fig. 2. Time-to-peak vs. D/Ω for simplified problem. Vertical axis scales time-to-peak to analytic value when $D/\Omega = 0$ as given in (40). Solid and dashed curves correspond to obliquity factor and Fokker-Planck approaches, respectively. The skewness of the distribution is correctly captured in the Fokker-Planck approach and results in pronounced differences in the time-to-peak.

time-to-peak to decrease. However, the rotation speed given in (44) depends on the diffusion rate through (46), slowing as the diffusion rate increases. At small values of diffusion, the slower speed of rotation is the dominant effect, causing an increase in the time-to-peak. At large values of diffusion, the decrease in ϕ_{Max} dominates, leading to a decrease in the time-to-peak.

In the Fokker-Planck approach, all of the previously discussed effects are present. Additionally, the skewness of the distribution is also captured. As first observed by Vajk [13], this effect is not present in the obliquity factor formulation. For any distribution of finite spread in ϕ, the portions of the distribution moving in the x direction diffuse more quickly than those portions moving obliquely to it due to the denominator present in (43). To see this effect, the following definitions are made.

$$n = \int_{-\pi}^{\pi} d\phi \ \phi f, \tag{56}$$

$$\langle\phi\rangle = \frac{1}{n}\int_{-\pi}^{\pi} d\phi \ \phi f, \tag{57}$$

$$\nu = \frac{1}{n}\int_{-\pi}^{\pi} d\phi \ \left(\phi - \langle\phi\rangle\right)^2 f, \tag{58}$$

$$s = \frac{1}{n}\int_{-\pi}^{\pi} d\phi \ \left(\phi - \langle\phi\rangle\right)^3 f, \tag{59}$$

where n is the density, $\langle\phi\rangle$ is the mean, ν is the variance, and s is the skewness for the distribution, f, which is computed using a numerical solution to the Fokker-Planck equation. The distribution is then plotted for seven different values of D/Ω in Fig. 3(a). The horizontal and vertical axes correspond to ϕ and f, respectively, where f is plotted at time, $\Omega\tau = 0.1$ with $v/c = 0.9$ as before. The tallest black curve corresponds to $D/\Omega = 0.1$, and the successive shorter ones, to $D/\Omega = 0.3$, 0.5, 0.7, 0.9, 1.1, and 1.3. As the diffusion increases, not only does the spread of f increase, but the distribution becomes

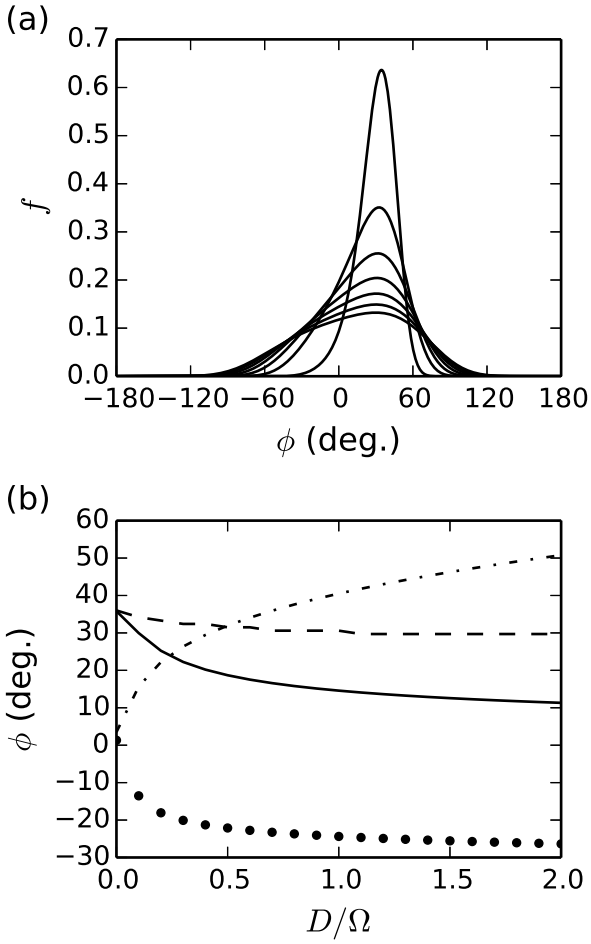

Fig. 3. Illustration of skewness of the distribution at $\Omega\tau = 0.1$, assuming $v/c = 0.9$. (a) Distribution function vs. ϕ for different values of D/Ω. From tallest to shortest, the curves correspond to $D/\Omega = 0.1$, 0.3, 0.5, 0.7, 0.9, 1.1, and 1.3, respectively. As the relative diffusion increases, the distribution becomes more skewed towards $\phi = 0$. (b) Plots characterizing the mean (solid), peak value (dashed), square root of the variance (dash-dotted), and cube root of the skew (dotted) vs. D/Ω. Skewness causes mean to lag behind peak value.

noticeably skewed towards $\phi = 0$. In the lower panel, Fig. 3(b), the quantitative measures given in (57) - (59) are plotted. The vertical and horizontal axes correspond to the value of the parameter plotted in degrees and the scaled diffusion, D/Ω, respectively. The solid, dash-dotted and dotted curves correspond to $\langle\phi\rangle$, $\nu^{1/2}$, and $s^{1/3}$, respectively, where the powers are introduced so that all quantities are measured in degrees. The dashed curve corresponds to the value of ϕ at which the peak value of the distribution occurs, ϕ_{Peak}. The discrepancy between ϕ_{Peak} and $\langle\phi\rangle$ is due to the skewness of the distribution. Because the skew creates a fat tail near $\phi = 0$, the skew is negative, causing the average value, the solid curve, to be below the peak value, the dashed curve.

Finally, it is useful to discuss the physical reason behind the increased scattering when electrons are traveling near the line of sight. For a fixed interval, $d\tau$, the amount of time elapsed and the distance through which a particle has traveled is given

by

$$dt = \frac{1}{1 - \frac{v}{c}\cos\phi} d\tau, \tag{60}$$

$$ds = \frac{v}{1 - \frac{v}{c}\cos\phi} d\tau. \tag{61}$$

In the above equations, it is clear that a particle traveling along the line-of-sight, $\phi \approx 0$, travels a longer distance, ds, over a larger amount of elapsed time, dt, than a particle traveling in an oblique direction. The greater amount of elapsed time allows for more collisions to occur, spreading the distribution more quickly near $\phi = 0$. This leads to the skewness which is ultimately observed.

IV. Full Problem

The understanding developed in the previous section is now applied to the full problem as presented in Sec. II. The problem is solved numerically using both the obliquity factor approach and a finite difference scheme. The numerical approaches are outlined in Subsec. IV-A, and the results are presented in Subsec. IV-B.

A. Numerical Methods

The obliquity factor approach amounts to solving the coupled equations,

$$\frac{d}{d\left(\Omega_0\tau\right)}\left(\frac{\mathbf{p}}{mc}\right) = \frac{1}{1 - \frac{v_z}{c\eta}}\left[\hat{\mathbf{B}} \times \frac{\mathbf{p}}{mc\gamma} - \kappa\hat{\mathbf{p}}\right], \tag{62}$$

$$\frac{d\eta}{d\left(\Omega_0\tau\right)} = \frac{2}{1 - \frac{v_z}{c\eta}}\Lambda, \tag{63}$$

where they have been presented in scaled form with the scaled drag and scattering coefficients, κ and Λ, given in (31) and (32), respectively. All quantities above are defined in Sec. II with the exception of $\hat{\mathbf{B}}$ and $\hat{\mathbf{p}}$, which are unit vectors in the direction of the magnetic field and momentum, respectively. The electrons are initialized with equal probability spacings in ψ and α, so that

$$\frac{\int_0^{\psi_j} \sigma_{KN}(\psi)\sin\psi d\psi}{\int_0^{\pi/2} \sigma_{KN}(\psi)\sin\psi d\psi} = \frac{1+2j}{2N_\psi}, \tag{64}$$

$$\alpha_k = \frac{2\pi}{N_\alpha}k, \tag{65}$$

where N_ψ and N_α are the number of grid points in the ψ and α coordinates, respectively, and j and k are the associated particle indices. The initial magnitude of the momentum is given by (19), resulting in the Cartesian components of the momentum vector, $p_x = p_0(\psi_j)\cos\alpha_k\sin\psi_j$, $p_y = p_0(\psi_j)\sin\alpha_k\sin\psi_j$, and $p_z = p_0(\psi_j)\cos\psi_j$. The initial obliquity factor for each electron is set to unity. The equations can then be solved using a Runge-Kutta method. As the electron slows, the expressions for the drag and scatter, (31) and (32), cease to be valid because they assume the momentum is sufficiently large. In the derivation of the scattering equation, the argument of the logarithm appearing in L_S is equal to $2/\theta_{Min}$, where θ_{Min} is the minimum angle by which an electron will be scattered without the nucleus being screened. For the expression for scattering to be valid, $\theta_{Min} \ll 1$, which for $Z = 7.2$, implies that $p/mc \gg 2.9 \times 10^{-2}$. For this reason, particles are discarded when $p/mc < 2.9 \times 10^{-2}$. Having solved the equations numerically, the current density can be computed at each time step as,

$$\mathbf{j} = -ecZn_iN_\gamma r_0^2 \sum_i W \frac{\mathbf{v}_i/\eta_i}{1 - \frac{v_{z,i}}{c\eta_i}}, \tag{66}$$

where $W = N_0/(N_\alpha N_\psi)$, and

$$N_0 = \int \frac{\sigma_{KN}(\psi)}{r_0^2}\sin\psi d\psi d\alpha. \tag{67}$$

For the finite-difference approach, grids in $\mu = \cos\psi$ and α are specified as,

$$\mu_j = \cos\left(\pi\frac{J+1-j}{J+1}\right), \tag{68}$$

$$\alpha_k = -\pi + \frac{2\pi}{K}\left(\frac{2k+1}{2}\right), \tag{69}$$

where $j = 0, 1, ..., J+1$ and $k = 0, 1, ..., K-1$, with $J \times K$ corresponding to the number of interior points. The non-uniform grid in μ is chosen as it more accurately resolves the initial Klein-Nishina distribution. This allows for fewer grid points while still maintaining accuracy. The grid in the momentum coordinate is determined by the grid in μ through,

$$p_l = p_0(\mu_l), \tag{70}$$

where the μ_l are values of the grid in μ for which $\mu > 0$ and $p_l/(mc) > 2.9 \times 10^{-2}$. The former condition is because the Compton electrons must initially be moving forward, and the latter condition, so that the Compton electron has enough momentum so that the scattering coefficient is valid. The distribution function is then specified on these grids at times, $\tau^m = m\Delta\tau$, where $\Delta\tau$ is the time step. Periodic boundary conditions are imposed on $\tilde{f}_{j,k,l}$ in the α coordinate so that $\tilde{f}_{-1,k,l} = \tilde{f}_{J-1,k,l}$ and $\tilde{f}_{J,k,l} = \tilde{f}_{0,k,l}$. The boundary condition in μ is difficult to include because of the singularity that appears at $\mu = \pm 1$ in (30). This is addressed by first observing that the points represented by $\mu = \pm 1$ must be independent of α. With this observation, an extrapolation can be used near the boundaries so that,

$$\tilde{f}_{0,k,l} = \frac{1}{K}\sum_k \left[\frac{\mu_2 - \mu_0}{\mu_2 - \mu_1}\tilde{f}_{1,k,l} - \frac{\mu_1 - \mu_0}{\mu_2 - \mu_1}\tilde{f}_{2,k,l}\right], \tag{71}$$

with a similar equation at the opposite boundary. The above procedure allows for well-behaved numerical solutions, but higher order extrapolations exhibited numerical instability. The initial distribution is given by (16), which in scaled form is,

$$\frac{\tilde{f}_{j,k,l}}{Zn_iN_\gamma r_0^2} = \begin{cases} \frac{2}{p_{l+1}-p_{l-1}}\frac{\sigma_{KN}(\mu_l)/r_0^2}{1-p_l\mu_j/mc\gamma_l} & \text{if } \mathrm{p_l = p_0(\mu_j)} \\ 0 & \text{otherwise} \end{cases}. \tag{72}$$

In implementing the finite-difference scheme, the derivatives in μ and α are represented by centered differences of second order accuracy, and the derivative in p is represented by a first order, upwind difference. This takes the form,

$$\frac{\partial\tilde{f}_{j,k,l}}{\partial\tau} = \sum_{n,p} A_{jn,kp,l}\tilde{f}_{n,p,l} + \sum_n B_{ln}\tilde{f}_{j,k,n}, \tag{73}$$

with A corresponding to the derivatives in μ and α, and B, to the derivative in p. Operator splitting is used to decouple the motion in p from the motion in μ and α. Combining operator splitting with a second order, Crank-Nicholson procedure leads to two implicit equations that must be solved at each time step,

$$\left(I - \frac{\Delta\tau}{2}A_{jn,kp,l}\right)\tilde{f}^{m+\frac{1}{2}}_{n,p,l} = \left(I + \frac{\Delta\tau}{2}A_{jn,kp,l}\right)\tilde{f}^{m}_{n,p,l}, \tag{74}$$

$$\left(I - \frac{\Delta\tau}{2}B_{l,n}\right)\tilde{f}^{m+1}_{j,k,n} = \left(I + \frac{\Delta\tau}{2}B_{l,n}\right)\tilde{f}^{m+\frac{1}{2}}_{j,k,n}. \tag{75}$$

The centered differences in μ and α are sufficient so long as the actual diffusion dominates over numerical diffusion in the solution, and this is equivalent to requiring that the Péclet number for the equation not be too large. For the equation of interest, the Péclet number is defined as

$$\mathrm{Pe} = 2\frac{\Omega}{D} = 3.37\times 10^{19}\frac{B(\mathrm{Gauss})}{n_i(\mathrm{cm})}, \tag{76}$$

where the numerical factor is determined for the most energetic electrons generated by a gamma energy of four times the electron rest mass. At 30 km altitude, $\mathrm{Pe} = 22$, which is typical of the largest vaues considered in this manuscript. For this Péclet number, stability concerns require at least 22 grid points in μ, but the requirement for resolving the Klein-Nishina distribution is much greater. Thus, the resolution required for accuracy is more stringent than stability requirements unless elevations with ion densities smaller by at least an order of magnitude are considered. The case of negligible diffusion and drag, i.e., large Péclet number, is solved semi-analytically via the method of characteristics in the Appendix.

B. Results

Before solving the general problem, a simpler problem is first considered in which drag is neglected, but the shape of the initial distribution is varied. This is done in order to generalize the results in Section III to three dimensions and to probe the dependence of the results on the initial variance of the distribution. The initial distribution is defined by a ring of electrons launched with an initial velocity of $v/c = 0.9$ and polar angle, ψ_0. This choice is made so that the initial transverse current, j_x, is zero, but the variance, $\langle\psi^2\rangle$, varies. The momentum dependence of the scatter is ignored and is independently set to $D/\Omega = 1.0$. The time-to-peak for both the obliquity factor and the Fokker-Planck approach are plotted in Fig. 4. The horizontal axis corresponds to the initial polar angle of the distribution as measured in degrees, and the vertical axis to the rise time measured by the dimensionless parameter, $\Omega\tau$. The solid curve is computed using the obliquity factor, and the dashed curve, using the Fokker-Planck method. The obliquity factor initially peaks sooner than the Fokker-Planck approach, which is similar to the results shown in considering the two-dimensional model problem. However, as the cone angle increases, this situation is reversed. From this, it is apparent that the relative peaking of the two currents depends heavily on the initial distribution used.

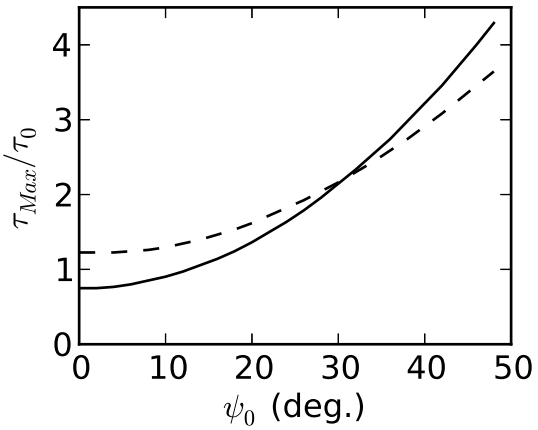

Fig. 4. Time to peak for the transverse current of electrons forming a ring in momentum space with velocity $v/c = 0.9$ and polar angle ψ_0 as measured from the z-axis. Solid and dashed curves correspond to the obliquity factor and Fokker-Planck methods, respectively. As the cone angle increases, the two curves cross, indicating that the relative peaking of the two methods depends on the initial distribution.

The numeric procedures are next applied to several cases outlined in [8], which implement all of the physics outlined in Sec. IV-A. A mono-energetic gamma spectrum of $E_\gamma = 1.6$ MeV is assumed with a geomagnetic field of $B = 0.6$ Gauss. Three different altitudes are considered: 30 km, 20 km, and ground. These correspond to number densities of $n_i(\mathrm{cm}^{-3}) = 7.53\times 10^{17},\ 3.68\times 10^{18}$, and 5.12×10^{19}, respectively. These values are determined from [18] with the average atomic mass of the atmosphere assumed to be $A = 14.4$. Further, analytic expressions for the initial slope of the transverse current and the initial value of the axial current are used as a check on the solutions. These are given by (36)-(39) of [8]; however, in (38), the last term in the square brackets possesses a typographical error and should have an additional factor of γ in the denominator. Finally, the procedure outlined in the Appendix is used to determine the vacuum solution for the Compton current.

Figure 5 depicts the transverse current at the altitudes: 30 km, 20 km, and ground. The vertical axes in each figure are the transverse current, j_x, scaled to $N_0 ec$, where N_0 is the number of Compton electrons produced by the gamma pulse at $\tau = 0$. The horizontal axes represent τ in seconds. The top panel, Fig. 5(a), corresponds to Figs. 6 and 7 in [8], and use a similar presentation for easy comparison. The straight blue line is the theoretical initial slope of the transverse current. The bottom panel, Fig. 5(b), corresponds to the current at ground. The red dash-dotted, dashed, and solid curves are the vacuum result, the Fokker-Planck solution, and the obliquity factor solution, respectively, with the altitudes labeled on the figure.

Figure 6 plots the axial current corresponding to the same altitudes in Fig. 5. The vertical axis is the axial current, j_z, scaled to $N_0 ec$. The plot corresponds to Fig. 10 in [8] and the horizontal blue line is the initial value of the axial current as given in the same reference. The red dashed and solid curves are the the Fokker-Planck and obliquity factor solutions,

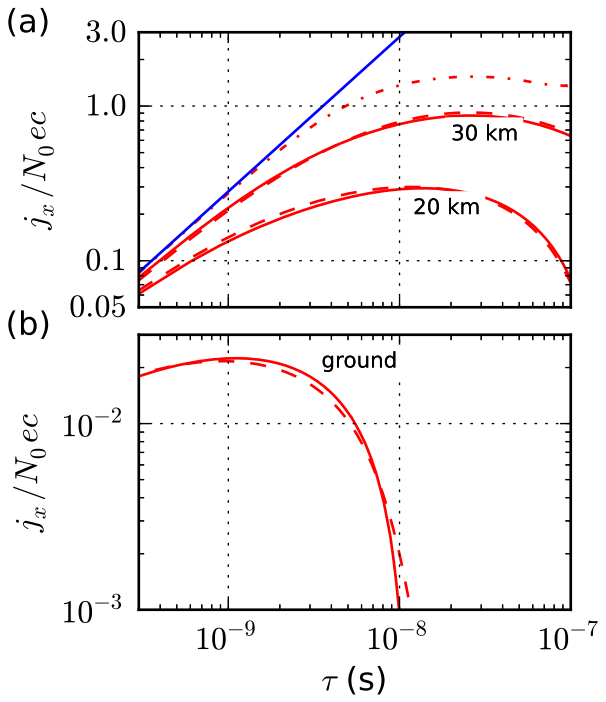

Fig. 5. Transverse Compton current at various altitudes for $E_\gamma = 1.6$ MeV and $B = 0.6$ Gauss. (a) 30 km and 20 km results. Corresponds to Figs. 6 and 7 of [8]. (b) Ground level. Blue lines correspond to theoretical initial slope. Dash-dotted curve corresponds to vacuum solution as given in Appendix. Solid and dashed curves correspond to obliquity factor and Fokker-Planck solutions, respectively.

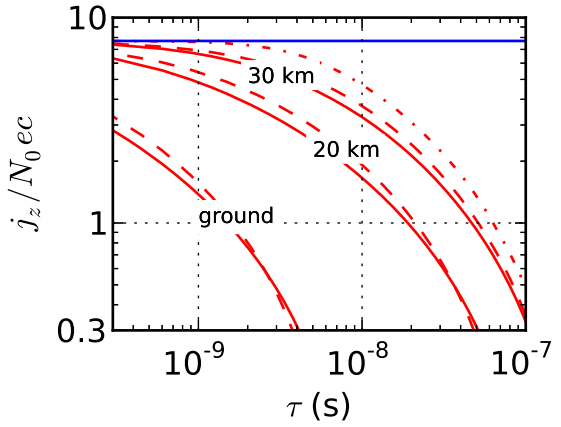

Fig. 6. Axial Compton current for cases shown in Fig. 5. Solid blue horizontal line corresponds to theoretical initial value of the axial Compton current. Dash-dotted curve corresponds to vacuum solution as given in Appendix. Solid and dashed curves correspond to Fokker-Planck and obliquity factor solutions, respectively, for 30 km, 20 km, and ground as labeled.

respectively. The altitudes are labeled on the figure.

Comparing these figures to those in [8], the Fokker-Planck results agree well with the previous Monte-Carlo studies. Further, the obliquity factor exhibits only small quantitative differences from the Fokker-Planck solution. The time-to-peak

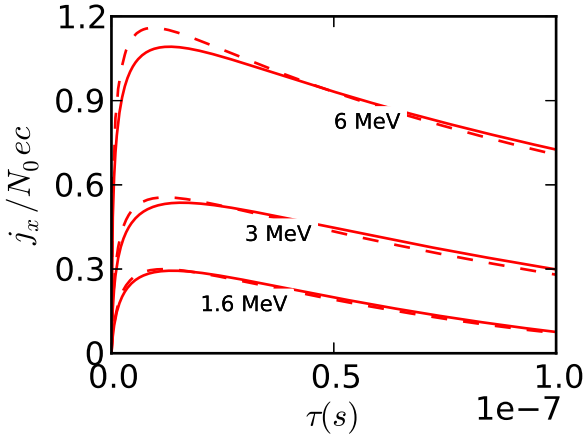

Fig. 7. Transverse Compton current for gamma energies of 1.6 MeV, 3 MeV, and 6 MeV at 20 km. The 1.6 MeV case corresponds to Fig. 5. The 3 MeV and 6 MeV cases used B = 0.5 Gauss. Solid and dashed curves correspond to the obliquity factor and Fokker-Planck solutions, respectively.

values agree within 2% and the maximum current values, within 5%. This agreement is present in both the source region (20 - 40 km) and extends to the ground. It is also observed that the Fokker-Planck solutions actually peak slightly earlier than the obliquity factor. This is attributed to the broadness of the initial distribution and the influence of drag reducing the peak of the signal.

In light of the results of Sec. III, it is perhaps surprising that the two methods agree so well. In choosing 1.6 MeV gamma photons, the initial variance of the distribution is quite large. This reduces the impact of skewness on the distribution, because the broad variance dominates the dynamics. To verify this explanation, two cases were examined. In the first, the gamma energy is varied so that the distribution becomes more peaked in the forward direction. The transverse current for such a case is plotted in Fig. 7 for the gamma energies, 1.6 MeV, 3 MeV, and 6 MeV, at an altitude of 20 km. The 1.6 MeV case is the same case as shown in Fig. 5, whereas the 3 MeV and 6 MeV cases used a background magnetic field of 0.5 Gauss. The horizontal axis corresponds to time as measured from the passage of the gamma pulse, and the vertical axis, to the scaled Compton current, j_x/N_0ec. The solid curves and dashed curves correspond to the obliquity factor and Fokker-Planck solutions, respectively. In all cases, the Fokker-Planck Compton current peaks before the obliquity factor solution. This is attributed to the use of the Klein-Nishina distribution. Additionally, as the energy of the gamma photons is increased, the discrepancy between the two methods also increases. In the 6 MeV case, the Fokker-Planck Compton current peaks 4 ns earlier, and the magnitude of the Compton current increases by 6%.

A second test was performed in which the angular spread of the Klein-Nishina distribution was ignored and all electrons are launched in the forward direction (or along the z-axis). The transverse currents are shown in Fig. 8. The axes are the same as in the previous figure. For both panels, the gamma energy is 1.6 MeV and the background magnetic field is 0.6 Gauss.

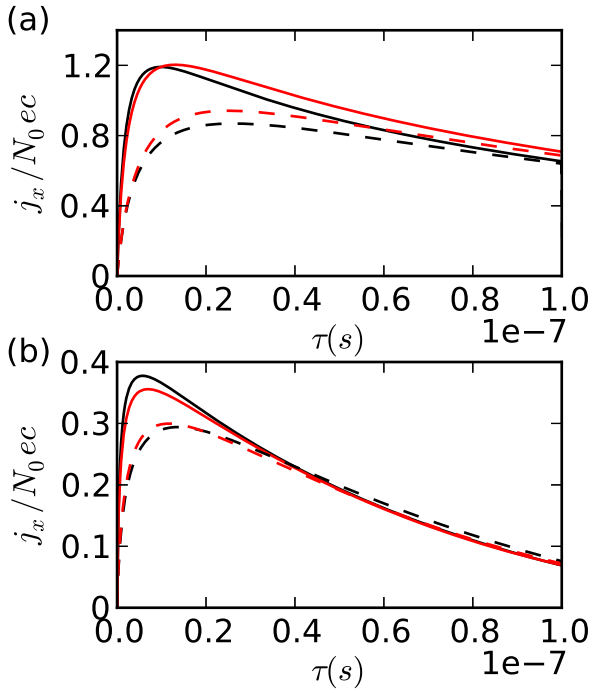

Fig. 8. Transverse Compton current for gamma energy, 1.6 MeV, at a magnetic field of 0.6 Gauss; (a) 30 km altitude, (b) 20 km altitude. Sold curves correspond to forward-launched electrons, and dashed curves, to using the angular spread of the Klein-Nishina distribution. Red and black curves correspond to Fokker-Planck and obliquity factor solutions, respectively. Obliquity factor peaks before the Fokker-Planck solution in the forward-launched case. This situation reverses when full angular spread is considered.

The solid and dashed curves correspond to launching along the z-axis and to using the full Klein-Nishina distribution, respectively. The red and black curves correspond to the Fokker-Planck and obliquity factor solutions, respectively. The top panel, Fig. 8(a), corresponds to an active region at 30 km altitude, and the bottom panel, Fig. 8(b), 20 km. Note that at this level of description the location of the gamma source does not enter into the calculation. In the forward-launched case, the Fokker-Planck solution peaks later than the obliquity factor solution. The results suggest that skewness (and other higher order effects) not contained in the obliquity factor formulation are small effects when the full Klein-Nishina distribution is considered.

V. Discussion and Conclusions

This analysis has demonstrated that the Doppler effect created by the spiraling Compton electrons leads to a skewness of the distribution in the τ coordinate. In the model problem that excludes drag, a significant discrepancy exists between the obliquity factor approach and both a Monte-Carlo and a Fokker-Planck description of the collisions. This shows that the early criticisms given by Vajk [13] have merit. However, in applying the Fokker-Planck description developed here to the full problem, agreement is found with earlier analysis performed by Longmire [8], and his principal conclusion that the obliquity factor is a good description of multiple scattering is verified. This is attributed to the broad spread of the Klein-Nishina distribution and would not occur for a narrower initial distribution. Further, as the gamma energy increases and the initial distribution becomes increasingly peaked in the forward direction, the accuracy of the approximation decreases. In all cases which considered the full angular spread of the Klein-Nishina distribution, the Fokker-Planck solutions peaked sooner than the obliquity factor, indicating that a proper description of multiple scattering would not lead to an increase in the rise time of the currents.

The impact of a more complete scattering treatment on full EMP modeling was assessed previously in HEMP [12]. Because a conductivity model has not been included in our study, direct comparisons to those results are not possible. In recent work, Kruger suggests that properly including multiple scattering in the description of the Compton electrons would increase the rise-time of the EMP fields observed in legacy codes (and thus, lower the frequency content) [14]. The results of this paper bear on the generation of the Compton current and not the electric field, and any direct comparison to [14] must await further analysis with a more complete model.

The obliquity factor was first introduced as an elegant simplification that allowed the EMP problem to be modeled using the computational resources that existed at the time. Further, the obliquity factor can be viewed as a valid zeroth order approximation of a fuller physics model. The results reported here combined with Longmire's earlier studies [8] show that the obliquity factor describes the transverse current (which excites the radiated electric field) reasonably well and is adequate for most purposes.

Appendix

If the effects of collisions are neglected, (30) reduces to an advection equation of the form,

$$\left(1-\frac{p}{mc\gamma}\cos\psi\right)\frac{\partial\tilde{f}}{\partial\tau}+\Omega\left[\frac{\cos\psi}{\sin\psi}\sin\alpha\frac{\partial\tilde{f}}{\partial\alpha}-\cos\alpha\frac{\partial\tilde{f}}{\partial\psi}\right]=0, \tag{77}$$

where the equation has been expressed in the angular coordinates, ψ and α. This can be solved via the method of characteristics by defining each variable to depend on the auxiliary variable, t. If this is done, the partial differential equation reduces to the set of ordinary differential equations,

$$\frac{d\tau}{dt}=1-\frac{p}{mc\gamma}\cos\psi(t), \tag{78}$$

$$\frac{d\alpha}{dt}=\Omega\cot\psi(t)\cos\alpha(t), \tag{79}$$

$$\frac{d\psi}{dt}=-\Omega\cos\alpha(t), \tag{80}$$

$$\frac{d\tilde{f}}{dt}=0. \tag{81}$$

The initial condition for $\tilde{f}$ is

$$\tilde{f}(t=0)=\tilde{f}_0=\frac{Zn_iN_\gamma}{1-\frac{p}{mc\gamma}\cos\psi}\delta(p-p_0(\psi))\sigma_{KN}(\psi), \tag{82}$$

The solution is,

$$\tilde{f} = \frac{Zn_i N_\gamma}{1 - \frac{p}{mc\gamma}\cos\tilde{\psi}} \delta(p - p_0(\tilde{\psi}))\sigma_{KN}(\tilde{\psi}), \tag{83}$$

$$\cos\tilde{\psi} = \cos\psi\cos\Omega t - \sin\psi\cos\alpha\sin\Omega t, \tag{84}$$

$$\Omega\tau = \Omega t + \frac{p}{mc\gamma}\left[\sin\psi\cos\alpha\left(1-\cos\Omega t\right) - \cos\psi\sin\Omega t\right]. \tag{85}$$

Here, $\tilde{\psi}$ represents the initial polar angle at $\tau = 0$. At later τ, the solution is advected to position (ψ,α) from the initial position. To determine the current,

$$\mathbf{j} = -eZn_i cN_\gamma r_0^2 \int \frac{p_0(\tilde{\psi})/mc}{\gamma(\tilde{\psi}) - \left(p_0(\tilde{\psi})/mc\right)\cos\tilde{\psi}} \times \frac{\sigma_{KN}(\tilde{\psi})}{r_0^2}\left[\cos\psi\hat{\mathbf{z}} + \sin\psi\cos\alpha\hat{\mathbf{x}}\right]\sin\psi d\psi d\alpha, \tag{86}$$

where the dependence on the magnitude of the momentum has been integrated. To compute the above expression, both $\tilde{\psi}$ and τ are determined parametrically on a grid in t. An interpolation is then performed onto the desired grid in τ, and the integrand that appears in the expression for the current density can be evaluated. Because the integral in p has been performed, the function $\tau(t)$ becomes multiple-valued. For this reason, care must be taken in performing the interpolations by dividing $\tau(t)$ into monotonic intervals and summing the interpolated value of the integrand in each interval. The integral is then performed numerically, and the current density is evaluated.

ACKNOWLEDGMENT

The authors are grateful to B. I. Cohen, C. D. Eng, H. W. Kruger, D. J. Larson, and D. P. Grote for helpful discussions regarding the material and for suggestions that have improved the content of this manuscript. This work was supported by the U.S. Department of Energy by Lawrence Livermore National Laboratory under Contract DE-AC52-07NA27344.

REFERENCES

[1] C. L. Longmire, *Close in E. M. Effects Lectures X and XI* (LAMS 3073). Los Alamos, NM: Los Alamos Scientific Lab, Apr. 1964.

[2] C. L. Longmire and H. J. Longley, "Improvements in the treatment of compton current and air conductivity in EMP problems," *Defense Nuclear Agency*, Alexandria, VA, Rep. DNA-3192T, Oct. 1973.

[3] C. L. Longmire, "On the electromagnetic pulse produced by nuclear explosions," *IEEE Trans. Electromagn. Compat.*, vol. EMC-20, no.1, p. 3, 1978.

[4] C. L. Longmire, "Justification and verification of high-altitude EMP theory Part I," Lawrence Livermore National Laboratory, Livermore, CA, Rep. UCRL-15938, Aug. 1987.

[5] W. J. Karzas and R. Latter, "Electromagnetic radiation from a nuclear explosion in space," *J. Geophys. Res.*, vol. 67, no. 12, pp. 4635-4640, Nov. 1962.

[6] W. J. Karzas and R. Latter, "Detection of the electromagnetic radiation from nuclear explosions in space," *Phys. Rev.*, vol. 137, no. 5B, pp. 1369-1378, Mar. 1965.

[7] H. J. Longley and C. L. Longmire, "Devlopment of the CHAP EMP Code," Defense Nuclear Agency, Alexandria, VA, Rep. DNA-3150T, Jan. 1972.

[8] C. L. Longmire, "Effect of multiple scattering on the compton recoil current," *Mision Research Corp.*, Santa Barbara, CA, Rep. MRC-R-378, Feb. 1978.

[9] G. R. Knutson, "Effect of nuclear-coulomb electron scattering on high altitude EMP sources," Air Force Weapons Laboratory, EMP Theor. Note 161, 1972.

[10] G. R. Knutson, "Treatment of electron scattering and approximate methods used for specifying high-altitude EMP sources," Air Force Weapons Laboratory, EMP Theor. Note 204, 1973.

[11] C. L. Longmire, "The early-time EMP from high-altitude nuclear explosions," *Mission Research Corp.*, Santa Barbara, CA, Rep. MRC-R-809, DNA-TR-84-175, Dec. 1983.

[12] W. E. Page, C. W. Jones, and R. L. Knight, "Electromagnetic pulse environment studies: a description of the HEMP-B computer code," Air Force Weapons Laboratory, 1974.

[13] J. P. Vajk, "Critique of compton current models used in high altitude EMP computer codes," Lawrence Livermore Laboratory, Report UCRL-77860, Dec. 1975.

[14] H. Kruger, "3D effects in geomagnetic EMP computations," *J. Rad. Eff.*, vol. 31, no. 1, pp. 159-170, Feb. 2013.

[15] X-5 Monte Carlo Team, "MCNP - a general Monte Carlo N-particle transport code, version 5," Los Alamos National Laboratory, Report LA-UR-03-1987, April 2003.

[16] M. N. Rosenbluth, W. A. MacDonald, and D. L. Judd, "Fokker-Planck equation for an inverse-square force," *Phys. Rev.* vol. 107, no. 1, pp. 1-6, Jul. 1957.

[17] A. P. L. Robinson, D. J. Strozzi, J. R. Davies, L. Gremillet, J. J. Honrubia, T. Johzaki, R. J. Kingham, M. Sherlock, and A. A. Solodov, "Theory of fast electron transport for fast ignition," *Nucl. Fusion* vol. 54, no. 5, pg. 4003, May 2014.

[18] *U.S. Standard Atmopshere*, National Oceanic and Atmospheric Administration, U.S. Government Printing Office, Washington D. C., 1976.